Chapter 1

HYDROGEN WALLS: MASS LOSS OF DWARF STARS AND THE YOUNG SUN

Jeffrey L. Linsky
JILA, University of Colorado and NIST
Boulder, CO 80309-0440 USA
jlinsky@jila.colorado.edu

Brian E. Wood
JILA, University of Colorado and NIST
Boulder, CO 80309-0440 USA
woodb@origins.colorado.edu

Abstract Charge-exchange reactions between a fully ionized stellar wind and the partially ionized warm gas in the interstellar medium create a compressed region of hot neutral hydrogen atoms that are decelerated relative to the inflowing interstellar gas. This "hydrogen wall" produces a blue-shifted absorption component in the stellar Lyman-α emission line at many viewing angles that has now been detected in *Hubble Space Telescope* spectra of eight dwarf stars. Comparisons of the observed Lyman-α line profiles with theoretical models led to the first sensitive measurements of mass-loss rates as small as 4×10^{-15} $M_{\odot}$ yr^{-1} for solar-like dwarfs. Our study of astrospheres provides the first observational data (other than for the Sun) with which to test theories for dwarf star winds. We find an empirical correlation of stellar mass-loss rate with X-ray surface flux that allows us to predict the mass-loss rates of other stars and to infer the solar wind mass flux at earlier times, when the solar wind may have been as much as 1000 times stronger than at present. We mention some important ramifications for the history of planetary atmospheres in our solar system, that of Mars in particular, and for exoplanets.

1. Is the Solar Wind Unique?

The presence of blue-shifted absorption features in spectral line profiles convinced stellar spectroscopists in the early twentieth century that luminous stars must lose mass. The classic P Cygni line profile, which is typically seen in hot star spectra, consists of blue-shifted absorption and red-shifted emission. Observations of this profile provide clear evidence that a star is losing mass and that the expanding outer atmosphere is comparable to or larger than the stellar photosphere. Novae and supernovae demonstrate that mass loss can be very rapid at times. In a classic study of the α Her triple system, Deutsch (1956) measured the mass-loss rate of $\dot{M} \geq 3 \times 10^{-8} M_{\odot}$ yr^{-1} from the M5 giant in the system by analysis of absorption features superimposed on the spectrum of the G5 dwarf lying behind the wind of the M5 giant. This mass-loss rate, which is low compared to typical M supergiants, is nonetheless at least a factor of 10^6 times larger than the mean solar mass-loss rate of $2 \times 10^{-14} M_{\odot}$ yr^{-1}. Lamers & Cassinelli (1999) have reviewed the observational evidence and theoretical models proposed to explain the mass loss from luminous hot and cool stars.

Stellar mass loss plays important roles in astrophysics including: (i) chemically enriching the interstellar medium out of which the next generation of stars emerges, (ii) exposing to view the chemically processed material in the inner layers of rapidly mass-losing stars (e.g., Wolf-Rayet stars), and (iii) changing the evolution of stars that lose a large portion of their mass either when young or in their post-main sequence phases, especially in the asymptotic giant branch phase of their evolution.

Biermann (1951) first showed that the Sun loses mass based on observations that comet plasma tails always face away from the Sun. Parker (1958, 1960) predicted that the Sun should have a high-velocity outflow, which is driven by the thermal gas pressure of the hot corona. To describe this outflow he coined the term "solar wind". Subsequent measurements of solar wind properties *in situ* using instruments on many satellites, most recently by *Ulysses* in its journey over the solar poles, demonstrated that Parker was basically right. However, additional acceleration and heating by magnetic waves may play important roles. For example, the coronal magnetic field provides the structure and controls the speed and density of the solar wind. Transient events (e.g., coronal mass ejections) also play a role.

The *Ulysses* space probe is providing the first detailed three-dimensional picture of the solar wind from *in situ* measurements obtained over a wide range of solar latitudes and solar-cycle phases. The solar wind has at least three identified components, which are correlated with the local magnetic field structure. The solar wind properties obtained from analysis of the *Ulysses* data are summarized in Table 1.1 (Phillips et al. 1995 with mass-flux values updated from the

Ulysses/SWOOPS website[1]). For each coronal region the table lists the wind speed (v_∞) at the Earth, the ion density (n_{ion}) at the Earth, the mass-loss rate ($\dot{M}_{total}$) if the entire Sun consisted of this region, and the percent of the solar surface typically covered by this region at solar-cycle maximum and minimum. An important point is that there is less than a factor of two difference in the solar mass-loss rate between regions of open magnetic fields in coronal holes characterized by a high-speed but low-density wind and the largely (but not entirely) closed magnetic-field regions with their slow-speed but higher-density wind. The time-averaged contribution of coronal mass ejections to the solar wind is not well known but is likely of order 10%. Thus a sensible value for the mean solar wind mass-loss rate is about 2×10^{-14} solar masses per year, nearly independent of solar cycle phase. This may be compared with the mass-loss rates of 10^{-5} to 10^{-10} $\dot{M}_\odot$ yr^{-1} often cited for luminous cool stars. While the solar wind mass-flux rate is tiny by comparison with M supergiants, it can still play important roles in the evolution of solar-like dwarf stars as we shall see.

Table 1.1. Typical Parameters for the Three Components of the Solar Wind.

Region	v_∞ *(km s^{-1})*	n_{ion} *(cm^{-3})*	$\dot{M}_{total}$ *($10^{-14} M_\odot$ yr^{-1})*	*Coverage at solar (max, min)*
Open magnetic fields	700–800	2.7	1.5	20%, few %
Closed magnetic fields	≈ 400	7.0	2.6	$\approx$ 80%, $\approx$ 95%
Coronal mass ejections	≤ 1000	0.2	?	about 10%

If a middle-aged, relatively inactive star like the Sun has a wind, surely other dwarf stars with convective photospheres and presumably complex magnetic fields should also have winds. Until recently, proof of this assertion was considered impossible as there were no tools available to perform the measurements. There are no space probes available to make *in situ* measurements of plasma properties inside the winds of nearby stars, comets in other stellar systems are not visible, and blue-shifted absorption features are not seen in dwarf star spectra, presumably because their mass-loss rates are not very different from the Sun and thus are too small to provide significant opacity in stellar emission lines. High resolution spectra of the Fe XXI 1354 Å and Fe XII 1242, 1349 Å coronal emission lines observed in the UV spectra of solar-like dwarf stars by the *Goddard High Resolution Spectrograph (GHRS)* and *Space Telescope Imaging Spectrograph (STIS)* instruments on the *Hubble Space Telescope (HST)* (Ayres et al. 2003) show no Doppler shifts that would indicate outflowing coronal gas. High-resolution spectra of the coronal Fe XVIII 977 Å line observed with the

[1] http://swoops.lanl.gov/

FUSE satellite by Redfield et al. (2003) also show no Doppler shifts. Furthermore, *Chandra* observations of coronal emission lines have yet to provide any evidence for systematic Doppler shifts (relative to the stellar radial velocity) for solar-like dwarf stars (e.g., Ayres et al. 2001), indicating that the observed coronal gas is confined by strong closed magnetic fields rather than located in open field regions. Given these nondetections of stellar wind indicators, most astronomers would conclude that the winds of solar-like dwarf stars are unobservable.

If there were any chance of finding evidence for dwarf star winds, one might guess that the most optically-thick spectral line of the most abundant element might provide the clue. The Lyman-α line of atomic hydrogen, therefore, should be the place to look. It turns out that the Lyman-α line is the right place to look, but the path that led to the first evidence for dwarf star winds was not straightforward. In fact, nobody studied the Lyman-α line to search for stellar winds, but analyses of this line for a very different purpose revealed an important discrepancy that led to the discovery of winds by a fortuitous coincidence.

Resonance lines of atoms and ions that are abundant in the interstellar medium (ISM) contain absorption features produced by the ISM gas. Important examples include the H I Lyman-α, C II 1334 Å, O I 1302 Å, and Mg II 2796, 2803 Å lines in the ultraviolet, which could be observed with the high resolution echelle gratings on *GHRS* and can now be observed with *STIS*. Linsky et al. (1993, 1995) analyzed high resolution *GHRS* spectra to derive column densities of important interstellar ions located along the lines of sight to the nearby stars Capella and Procyon. The prime objective of this program was to infer the D/H ratio in the local ISM. When analyzing the next data set in this program, Linsky and Wood (1996) found a major discrepancy in the α Cen A and α Cen B data. For these two adjacent lines of sight, the central velocity of the H I Lyman-α absorption is –15.7 km s^{-1}, whereas the central velocities of the interstellar D I Lyman-α, Mg II 2796, 2803 Å and Fe II 2599 Å lines are –18.1 km s^{-1} within measurement errors (see Table 1.2). This 2.4 km s^{-1} difference is much larger than the expected errors in the *GHRS* wavelength scale. Also, the H I and D I Lyman-α lines are only 82 km s^{-1} apart and were observed at the same time. Thus the wavelength discrepancy cannot be instrumental in origin. Incidently, Landsman et al. (1984) also noticed a velocity discrepancy between the H I and D I Lyman-α lines in their *Copernicus* observations of α Cen A, but they did not have an explanation for this discrepancy.

We were able to fit the observed H I Lyman-α absorption feature with two components: one centered at the velocity of the other ISM lines with thermal and turbulent broadening consistent with them and the other componant redshifted by about 4 km s^{-1} from the ISM velocity. The second component has a column density a factor of 1,000 smaller than the ISM component and a broad profile indicating a temperature of about 27,000 K. We initially had no idea as to the origin of this second component, but its existence is nearly certain.

Table 1.2. Interstellar Parameters for α Cen Lines of Sight.

Star	*Ion*	*Line*	*Velocity* *(km s^{-1})*	*log N_{HI}*	τ
α Cen A	Fe II	2599.396	-18.2 ± 0.1	12.441 ± 0.004	1.64
α Cen A	Fe II	2599.396	-17.7 ± 0.1	12.445 ± 0.022	1.39
α Cen A	Mg II	2795.528	-18.1 ± 0.1	12.698 ± 0.017	5.50
α Cen A	Mg II	2802.705	-17.8 ± 0.1	12.691 ± 0.003	2.76
α Cen A	Mg II	2802.705	-17.8 ± 0.1	12.776 ± 0.010	3.35
α Cen B	Mg II	2795.528	-18.2 ± 0.1	12.640 ± 0.003	4.48
α Cen B	Mg II	2802.705	-18.0 ± 0.1	12.802 ± 0.003	3.61
α Cen A	D I	1215.339	-18.2 ± 0.1	12.779 ± 0.015	0.72
α Cen B	D I	1215.339	-18.2 ± 0.1	12.775 ± 0.009	0.65
α Cen A	H I	1215.670	-15.9 ± 0.1	18.031 ± 0.003	68700
α Cen B	H I	1215.670	-15.6 ± 0.1	18.027 ± 0.002	68100

Serendipity provided the missing explanation for the origin of the second component in the Lyman-α line. On July 11, 1995, a number of interesting papers were presented at Symposium 404 “The Local Interstellar Cloud and the Boundary of the Heliosphere”, which was a part of the IAGA General Assembly in Boulder Colorado. In oral presentations at this meeting, H.L. Pauls, G.P. Zank, and V.B. Baranov presented theoretical models for the interaction of inflowing ISM gas with the outflowing solar wind, including charge exchange reactions between protons and hydrogen atoms. In these models the interaction of the solar wind with the ISM gas produces enhanced hydrogen densities near and somewhat beyond the heliopause, producing the “hydrogen wall”. The neutral hydrogen in the wall is decelerated by a few km s^{-1} relative to the undisturbed ISM flow, is heated above the ISM temperature, and has a column density of a few times 10^{14} cm^{-2}. These are the same parameters that Linsky and Wood (1996) had inferred empirically for the second component in the Lyman-α line without knowing the physical origin of the absorption. Our realization at the meeting that the hydrogen wall can simply explain the extra absorption component provided the tool that would eventually lead to the first measurements of mass-loss rates from dwarf stars and to sensible estimates of mass-loss rates for the young Sun as a function of age.

2. Hydrogen Walls: A New Tool for Measuring Mass-Loss Rates

Figure 1.1 shows the Lyman-α emission line of α Cen B, the K2 V secondary star in the nearest stellar system to the Sun, which was observed by Linsky & Wood (1996) using the echelle-A grating of *GHRS* with a resolution of 3.6 km s^{-1}. Superimposed on the stellar emission line are two absorption features: the broad, saturated absorption feature centered near 1215.6 Å, which is produced mostly by interstellar neutral hydrogen (H I) and a narrow absorption feature centered near 1215.25 Å, which is produced by interstellar deuterium (D I). The upper solid line in the figure is our estimate of the intrinsic stellar Lyman-α emission line obtained by scaling the observed solar Lyman-α line profile and matching the far wings of the observed stellar emission line. The dashed line in Figure 1.1 is the Lyman-α emission remaining after interstellar absorption alone is considered, where the ISM H I absorption is forced to have the thermal broadening and centroid velocity consistent with that of D I. Excess absorption is clearly seen on both sides of the H I absorption feature. Linsky & Wood (1996) proposed that this excess absorption is produced by interstellar H I gas in the outer heliosphere that has been heated and Doppler shifted by its interaction with the solar wind.

This interpretation of the excess H I absorption has strong theoretical support from recent models of the heliosphere that include both the ionized plasma and neutral H atoms in a self-consistent manner. The first such self-consistent models were those of Baranov & Malama (1993, 1995). These were followed by other models such as those of Pauls et al. (1995) and Zank et al. (1996). The basic structure of the heliosphere is illustrated in Figure 1.2. The solar wind is decelerated to subsonic speeds at the termination shock, the ISM plasma is decelerated to subsonic speeds at the bow shock, and the heliopause between these two shocks separates the plasma flows of the ISM and the solar wind. The theoretical models show that charge exchange between protons and hydrogen atoms in the outer heliosphere lead to a population of hot H I gas that permiates the entire heliosphere, as shown in Figure 1.3. This hot H I is especially prominent in the high-density "hydrogen wall" region between the heliopause and the bow shock (the region in white in the left panel of Figure 1.3).

Gayley et al. (1997) used the H I absorption for the α Cen line of sight predicted by the models of Zank et al. (1996) to demonstrate that heliospheric H I absorption could successfully account for the excess H I absorption on the red side of the Lyman-α line (vertical lines in Figure 1.1) but not the excess absorption on the blue side (horizontal lines in Figure 1.1). Gayley et al. proposed that the blue side excess is due to "astrospheric" material surrounding α Cen, analogous to the heliospheric H I detected on the red side of the line. The various theoretical models predict that the heliospheric absorption should

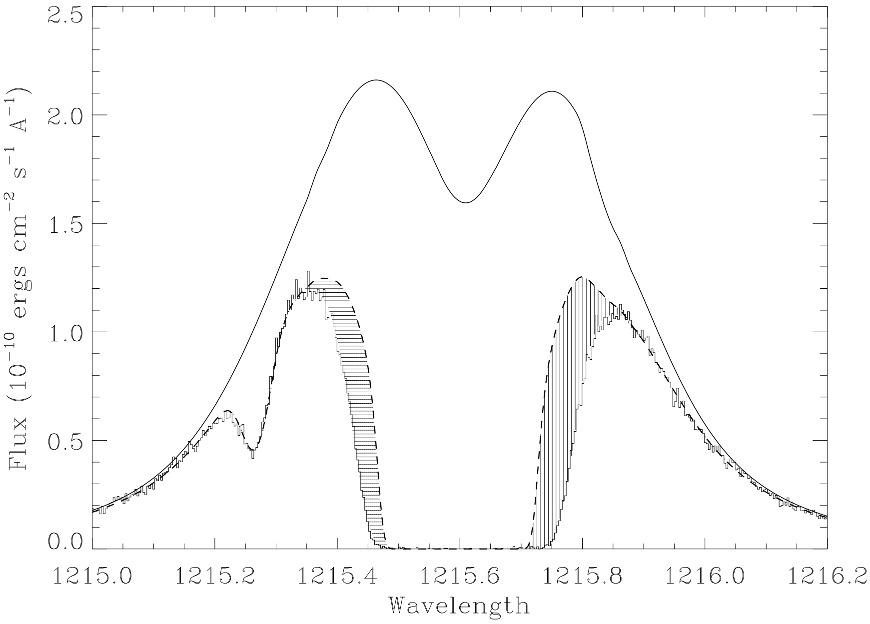

Figure 1.1. HST/GHRS Lyman-α line profile of α Cen B, showing broad H I absorption centered at 1215.6 Å and D I absorption centered at 1215.25 Å. The upper solid line is the assumed stellar emission line profile, and the dashed line is the effect of ISM absorption alone. The excess absorption is due to heliospheric H I (vertical lines) and astrospheric H I (horizontal lines).

be redshifted relative to the ISM absorption in all directions, mostly because of the deceleration and deflection of ISM gas as it crosses the bow shock, although other factors are at work in downwind directions (e.g., Izmodenov et al. 1999; Wood et al. 2000b). Conversely, astrospheric absorption should be blueshifted with respect to the ISM absorption for most observing angles, since we are observing the neutral hydrogen decelerated relative to the star from outside the astrosphere rather than from inside. Thus excess absorption on the red side of Lyman-α is best interpreted as heliospheric, while excess absorption on the blue side is most likely astrospheric.

Heliospheric absorption has now been reported for four lines of sight: α Cen (Linsky & Wood 1996), Sirius (Izmodenov et al. 1999), 36 Oph (Wood et al. 2000a), and Proxima Cen (Wood et al. 2001). Three other lines of sight (31 Com, β Cas, and ϵ Eri) observed by HST sample different orientation angles through the heliosphere and provide upper limits for the amount of heliospheric absorption that could be present in those directions (Wood et al. 2000b; Izmodenov et al. 2002).

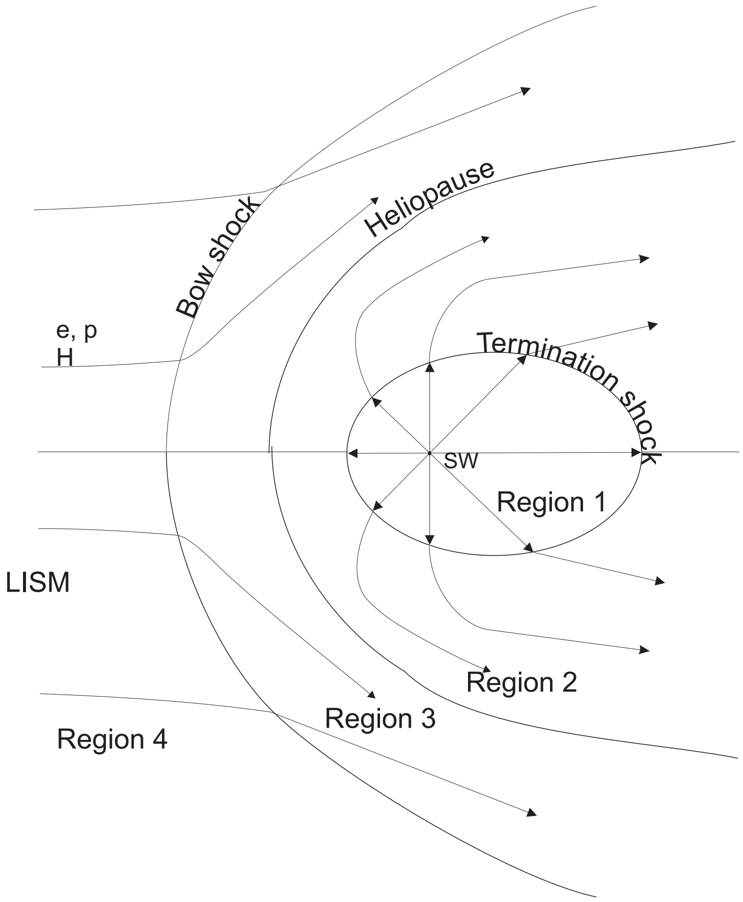

Figure 1.2. Schematic picture of the heliospheric interface, which can be divided into four regions, each with significantly different plasma properties as shown in the figure: (1) supersonic solar wind, (2) subsonic solar wind, (3) disturbed interstellar gas and plasma, and (4) undisturbed interstellar medium.

We show in Figure 1.4 the Lyman-α absorption profiles observed toward six of the seven stars mentioned above. We focus on the red sides of the profiles where the heliospheric absorption should be located. The θ angles given in the figure are the angles between the line of sight and the upwind direction of the interstellar flow. The six lines of sight sample a diverse range of orientation angles, from the nearly upwind direction toward 36 Oph ($\theta = 12°$) to the nearly downwind line of sight toward ϵ Eri ($\theta = 148°$). The dotted lines are the predicted Lyman-α profiles with only ISM absorption, for which the velocity and broadening parameters were obtained by fitting the D I absorption. Only 36 Oph, α Cen, and Sirius show excesses that reveal the presence of heliospheric

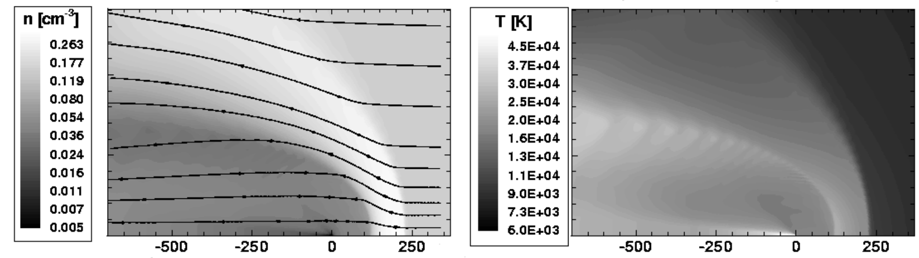

Figure 1.3. The H I density (left) and temperature (right) inside the heliosphere predicted by the Zank et al. (1996) hydrodynamic model of the ISM-solar wind interaction. The neutral hydrogen streamlines are shown in the left panel. The heliopause and bow shock are both visible at about 120 AU and 230 AU, respectively, in the upwind direction (i.e. on the right).

Table 1.3. Published Astrospheric Detections and Mass-Loss Measurements.

Star	*Spectral Type*	*d (pc)*	V_{ISM} *(km s^{-1})*	$\dot{M}$ *($\dot{M}_\odot$)*	*Sources*
α Cen	G2 V+K0 V	1.3	25	2	a,b,c
Prox Cen	M5.5 V	1.3	25	< 0.2	c
ϵ Eri	K1 V	3.2	27	30	d,j
61 Cyg A	K5 V	3.5	86	0.5	e,j
ϵ Ind	K5 V	3.6	68	0.5	f,g,h
36 Oph	K1 V+K1 V	5.5	40	15	i,j
ξ Boo	G8 V+K4 V	6.7	32	1	k
λ And[1]	G8 IV-III+	25.8	53	5	f,g,h

[1] Uncertain detection.

Sources: (a) Linsky & Wood 1996. (b) Gayley et. al. 1997. (c) Wood et al. 2001. (d) Dring et al. 1997. (e) Wood & Linsky 1998. (f) Wood et al. 1996. (g) Müller et. al. 2001a. (h) Müller et al. 2001b. (i) Wood et al. 2000a. (j) Wood et al. 2002. (k) Preliminary value.

absorption. A successful heliospheric model should reproduce accurately the amount of heliospheric absorption detected towards these three stars, while at the same time predicting no detectable absorption towards the other three stars. However, we have only begun to explore the potential that the HST data provide for testing the accuracy of heliospheric models, and for constraining the input parameters for these models that are poorly known observationally.

The predicted heliospheric H I absorption is very sensitive to the neutral hydrogen velocity distributions within the heliosphere. Unfortunately, the charge exchange processes in the outer heliosphere result in the hydrogen atoms being far from thermal equilibrium, and the velocity distributions are, therefore, far from Maxwellian (cf. Izmodenov et al. 2001). Ideally, a full kinetic treatment is

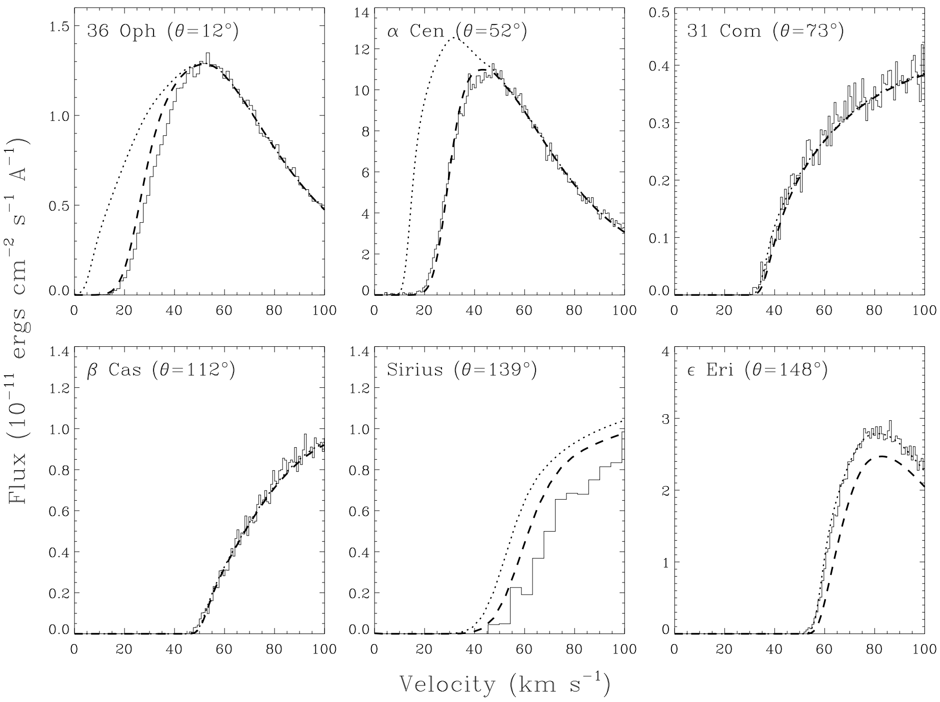

Figure 1.4. Comparison of the heliospheric H I absorption predicted by a four-fluid heliospheric model (dashed lines) and the observations, where the model heliospheric absorption is shown after having been added to the ISM absorption (dotted lines). Reasonably good agreement is observed, although there is a slight underprediction of absorption towards 36 Oph and Sirius, and a slight overprediction towards ϵ Eri. From Wood et al. (2000b).

required to accurately reproduce the distributions in such a situation. The models of Baranov & Malama (1993, 1995) and Müller et al. (2000) are examples of models that use a kinetic code to determine the neutral H properties. Wood et al. (2000b) used models computed with the Müller et al. (2000) code to predict absorption for comparison with the data in Figure 1.4. Despite assuming a range of values for the properties of the ISM surrounding the Sun, they were unable to find a model that is consistent with all of these lines of sight, mainly because the models predict too much absorption, especially in the downwind directions. Izmodenov et al. (2002) had somewhat better success with the kinetic models of Baranov & Malama (1993, 1995), but like Wood et al. (2000b) they also had problems with overpredicting the absorption in downwind directions.

Wood et al. (2000b) were able to find a so-called four-fluid model of the type described by Zank et al. (1996) that fits the heliospheric absorption data reasonably well. The model assumes the following ISM input parameters:

$n(H\ I) = 0.14$ cm^{-3}, $n(H^+) = 0.1$ cm^{-3}, and $T = 8000$ K. The predicted absorption from this model is also shown in Figure 1.4. Despite a slight over-prediction of absorption towards ϵ Eri and slight underpredictions for 36 Oph and Sirius, Wood et al. (2000b) argue that this four-fluid model fits the data acceptably well. The inclusion of magnetic fields in the solar wind and in the LISM can alter the heliosphere's shape (e.g., Linde et al. 1998) and thus the hydrogen wall absorption, perhaps leading to an explanation of the remaining discrepancies,

The four-fluid code of Zank et al. (1996) assumes that the hydrogen atoms can be treated as the sum of three distinct hydrodynamic fluids. (The fourth fluid is for the protons.) One would not expect that this approximation would lead to neutral H velocity distributions as accurate as those computed with codes that provide a full kinetic treatment for the neutrals, which make no assumptions about the shapes of H velocity distributions. Thus, the success of the four-fluid code in Figure 1.3 and the apparent failure of the kinetic codes are somewhat of a surprise. It is important to understand why the current kinetic codes have not been able to match successfully the observed heliospheric H I absorption, since kinetic codes should, in principle, produce more accurate velocity distributions. Further development of kinetic codes is required to determine whether or not more sophisticated kinetic codes can improve agreement with the data and lead to better estimates of ISM properties around the Sun.

Previous studies that used 2D models to predict heliospheric absorption assumed that the heliosphere is axisymmetric and the line of sight absorption is specified uniquely by the angle between the observed star and the upwind direction (θ in Figure 1.4). This approach is simplistic, because there are many effects that can change this conclusion, including latitudinal solar wind variations or a skewed orientation of the ISM magnetic field with respect to the ISM flow. The unstable jet sheet predicted by the models of Opher et al. (2003) is another example of a 3D effect that new generations of heliospheric models should include. The heliospheric absorption might provide important diagnostics for these effects. For example, if the magnetic field of the ISM is not perpendicular or parallel to the ISM flow, then the effective nose of the heliosphere could be shifted from the upwind direction (e.g., Ratkiewicz et al. 1998). It is possible that this shift would lead to changes in the distribution of heliospheric hydrogen that would be detectable in the Lyman-α absorption observations. However, in order for the HST data to be useful for studying 3D effects, many more lines of sight must be considered than the six in Figure 1.4, and more detections of heliospheric absorption must be found.

In our search of the HST archives conducted a little over a year ago, we found more than 40 lines of sight to stars within 100 pc of the Sun for which the observed Lyman-α line profiles had not yet been analyzed. (More distant lines of sight likely will have too much ISM absorption for heliospheric or

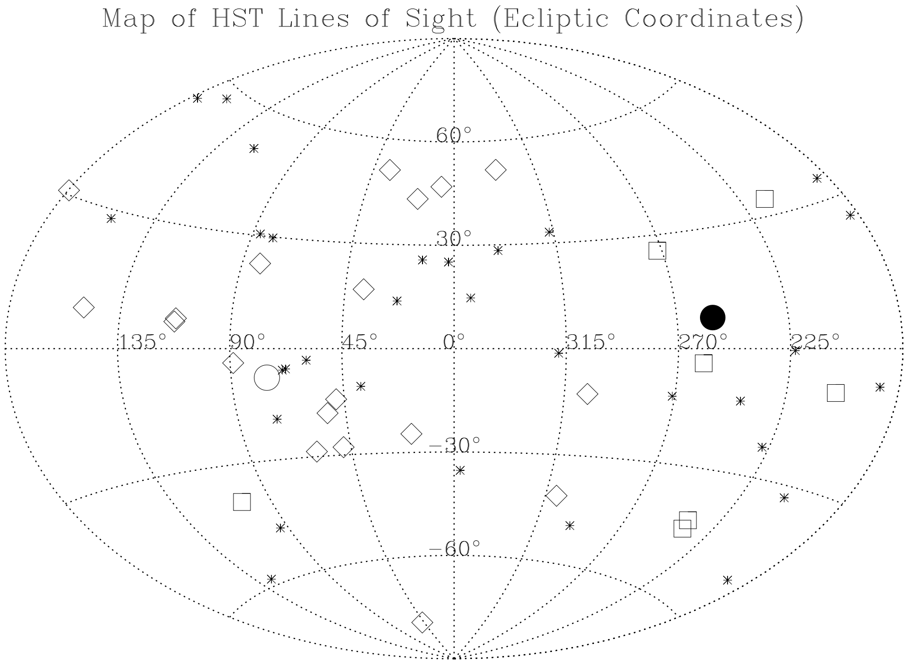

Figure 1.5. Sky map of HST-observed lines of sight in ecliptic coordinates, which have either yielded detected heliospheric Lyman-α absorption (boxes), nondetections of heliospheric absorption (diamonds), or have not yet been analyzed (asterisks). The filled and open circles are the upwind and downwind directions of the ISM flow as seen by the Sun.

astrospheric absorption to be detectable.) We have just begun to plow through the archival data, but we have already found three new heliospheric absorption detections and four new astrospheric detections. We show in Figure 1.5 a sky map of interesting HST-observed lines of sight in ecliptic coordinates. Boxes show lines of sight that have yielded detectable heliospheric absorption, while diamonds show nondetections. Six of the seven detections are near the upwind direction (identified by the filled circle). The heliospheric absorption is more easily detected in the upwind direction due to the substantial deceleration of hydrogen wall material, which redshifts the heliospheric absorption well away from the ISM absorption. The asterisks in the figure are lines of sight that will be analyzed in the near future.

2.1 Stellar Astrospheres

Not only has heliospheric H I been detected in HST data, but analogous astrospheric H I surrounding the stars has also been detected for some stars, as shown in Figure 1.1. The astrospheric absorption seen by HST represents the first detection, albeit indirect, of winds around other solar-like stars. Furthermore, the amount of absorption is a diagnostic for the stellar mass-loss rate, because the larger the mass-loss rate, the larger the astrosphere will be and the more Lyman-α absorption it will produce. Thus, mass-loss rates can be estimated from the astrospheric absorption, but as we will show below, the measurement process requires the computation of theoretical models analogous to the heliospheric models. Measurements of stellar mass-loss rates for stars of different ages and activity levels provides us with our very first opportunity to establish observationally how mass-loss rates vary with time for solar-like stars, including the Sun. Thus, measuring mass-loss rates from astrospheric absorption will allow us to determine the properties of the solar wind when the Sun was young.

The use of the four-fluid code of Zank et al. (1996) has already allowed significant progress in the estimation of stellar mass-loss rates from model fits to stellar Lyman-α line profiles. The first analysis was that of the α Cen astrospheric absorption (Wood et al. 2001), where the successful heliospheric four-fluid model from Wood et al. (2000b), as shown in Figure 1.6, was used in fitting the observed α Cen Lyman-α profile. To estimate the stellar mass-loss rate, one must first estimate the ISM wind vector seen by the star, by using the known stellar motion vector and the LISM flow vector. This vector is assumed to be the same as for the Local Interstellar Cloud (e.g., Lallement et al. 1995). These computations suggest that α Cen sees an interstellar wind speed of $V_{ISM} = 25$ km s^{-1}, almost identical to the 26 km s^{-1} velocity seen by the Sun (Witte et al. 1993). Our line of sight to α Cen is about $\theta = 79°$ from the upwind direction as seen by the star, so we are observing a sidewind portion of its astrosphere. In order to extrapolate from the successful heliospheric model mentioned above to an astrospheric model, we simply recompute the model assuming the stellar V_{ISM} value instead of the solar value while using the same values of the LISM density and hydrogen ionization. We then compute the astrospheric Lyman-α absorption for the line of sight described by the stellar value of θ. In order to experiment with different stellar mass-loss rates, we change the assumed stellar wind density.

The comparison of the Lyman-α profiles for Proxima Cen and α Cen B (see Figure 1.6) by Wood et al. (2001) provides an excellent example of heliospheric and astrospheric absorption. Since the two stars are only 2.2° apart in the sky and 1.3 pc distant from the Sun, the interstellar absorption (predicted from the deuterium and metal lines) and the heliospheric hydrogen wall absorption (on the red side of the interstellar absorption) should be the same. Indeed, the observations verify that this is the case.

On the other hand, the blue side of the Lyman-α absorption in the spectra of the two stars is different. Since this part of the absorption is due only to the astrospheric hydrogen wall absorption, the stellar winds of the two stars must

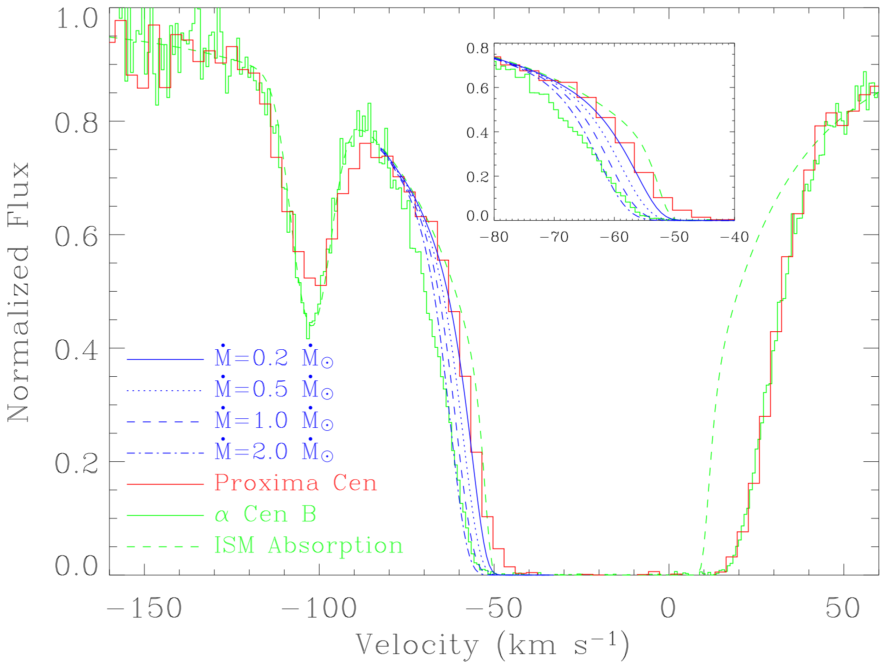

Figure 1.6. The α Cen B spectrum (thin solid line) and inferred ISM absorption (dotted line) from Figure 1.1. The dashed lines show the blue-side excess Lyman-α absorption predicted by four models of the α Cen astrosphere, assuming four different mass-loss rates. The 2.0 $\dot{M}_\odot$ model fits the α Cen spectrum reasonably well. The 0.2 $\dot{M}_\odot$ model is an upper limit for Proxima Cen. The insert shows an expanded view of the region of astrospheric absorption. From Wood et al. (2001).

be different. Comparison of such observations with theoretical models leads to estimates of the stellar mass-loss rate.

Figure 1.6 shows the α Cen B data compared with the astrospheric absorption predicted by four different models, with assumed mass-loss rates in the range $\dot{M} = 0.5$ to 2.0 $\dot{M}_\odot$. Since the $\dot{M} = 2\dot{M}_\odot$ model appears to fit the data best, we conclude that α Cen has about twice the mass-loss rate as the Sun. Since the α Cen binary separation is much smaller than the distance from the center of mass to the termination shock, both stars share the same astrosphere and the measured mass-loss rate represents the combined mass-loss rates of both α Cen A and α Cen B. Proxima Cen is separated from α Cen AB by at least 10^4 AU, so its astrosphere lies well outside of the astrosphere of α Cen AB and the two astrospheres are unlikely to interact. Note that the uncertainty in the inferred mass-loss rate due to possible errors in the assumed model parameters is minimized by extrapolating the astrospheric models from heliospheric

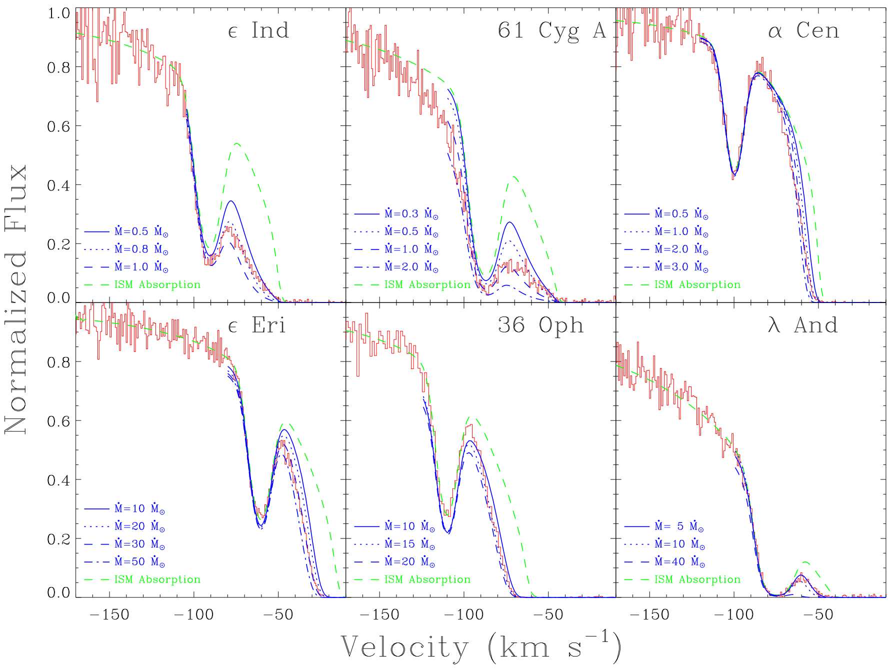

Figure 1.7. Closeups of the blue side of the H I Lyman-α absorption lines for all stars with detected astrospheric absorption, plotted on a heliocentric velocity scale. Narrow D I ISM absorption is visible in all the spectra just blueward of the saturated H I absorption. Green dashed lines indicate the interstellar absorption alone, and blue lines show the additional astrospheric absorption predicted by hydrodynamic models of astrospheres assuming various mass-loss rates.

models that fit the heliospheric Lyman-α absorption. In effect, the heliospheric absorption calibrates the models before they are applied to modeling astrospheres, and the mass-loss measurement technique is partially semi-empirical rather than purely theoretical. Figure 1.7 shows examples of our technique for estimating mass-loss rates for other stars by fitting the blue edge of the Lyman-α line absorption.

Table 1.3 lists the stars with published detections of astrospheric absorption. Mass-loss rates have been estimated for these stars using the method just described. The references in the table are to the papers that first reported the astrospheric detections and first presented mass-loss rate estimates. In Figure 1.8, we plot the mass-loss rates divided by the stellar surface area vs. the corresponding X-ray surface flux F_x (from Wood et al. 2002). For the solar-like G and K dwarfs, the data suggest that more active stars have higher mass-loss

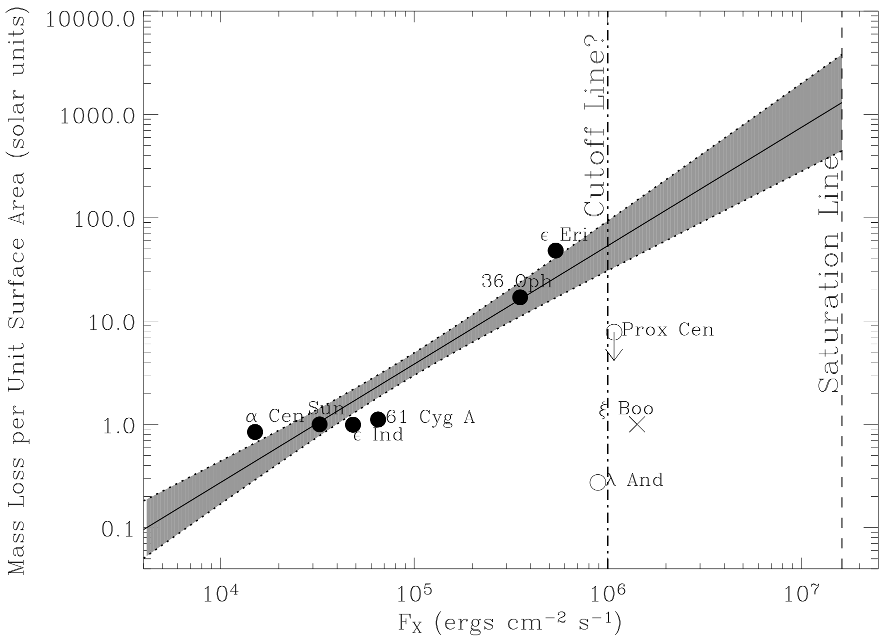

Figure 1.8. Measured mass-loss rates (per unit surface area) plotted versus X-ray surface flux (F_x). A power law has been fitted to the solar-like G and K dwarfs (filled circles) that excludes Prox Cen (M5.5 Ve) and λ And (G8 IV-III+M V). The preliminary ξ Boo (G8 V + K4 V) data point is inconsistent with the mass-loss/activity relation but is roughly consistent with Prox Cen and λ And, which suggests that the mass-loss/activity relation defined by the lower activity GK dwarfs may have a high activity cutoff (dot-dashed line). The saturation line represents the maximum F_x value observed for very active stars.

rates. The GK dwarf stars determine the mass-loss/activity relation, but the M dwarf Proxima Cen and the RS CVn system λ And (G8 IV-III+M V) are inconsistent with this relation. We had previously assumed that this was due to M dwarfs and RS CVn binaries having very different coronal structures than the GK dwarfs (Wood et al. 2002), but we have recently studied the astrosphere of the ξ Boo binary (G8 V + K4 V) by modelling the Lyman-α line in the *HST* archives. The preliminary mass-loss rate for ξ Boo (see Table 1.3) is consistent with the low mass-loss rates previously found for Proxima Cen and λ And. This new result calls into question our initial interpretation.

A common feature of ξ Boo, Prox Cen, and λ And is that they are all very active stars with X-ray surface fluxes near 10^6 ergs cm^{-2} s^{-1}, about a factor of 30 larger than the Sun. These three active stars all lie well below the GK star mass-loss/activity relation in Figure 1.8. Whereas we had previously assumed that Prox Cen and λ And were different types of stars than the GK dwarfs, both

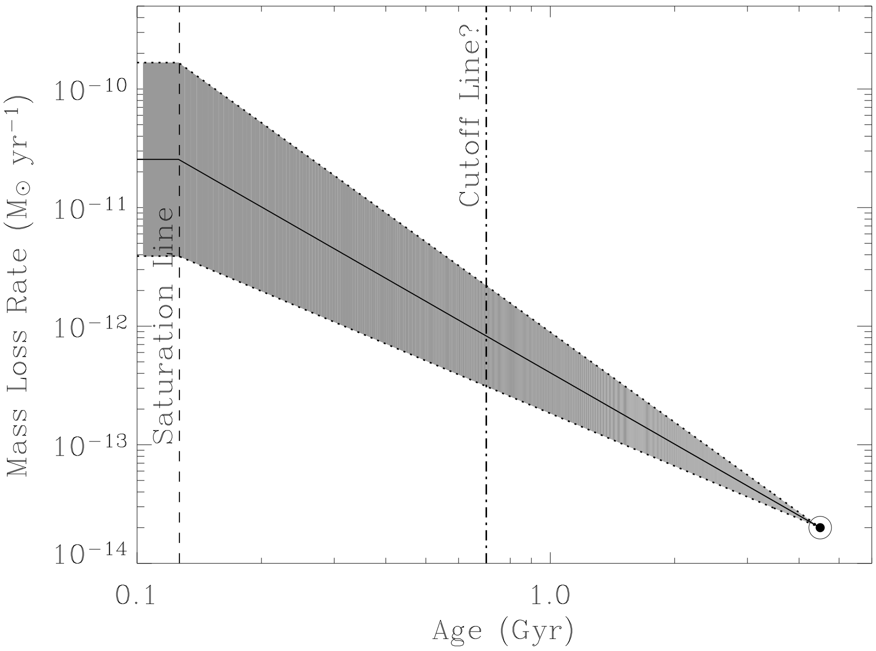

Figure 1.9. The mass-loss history of the Sun suggested by the power law relation (Equation 1.1) and the age/activity relation from Ayres (1997). If the high activity cutoff line is real, then the relation only applies for $t > 0.7$ Gyr.

stars in the ξ Boo system are normal G or K dwarfs. Thus the explanation for why ξ Boo, Prox Cen, and λ And lie below the previously determined relation for GK dwarfs could be their high activity. We suggest that there may be a high-activity cutoff to the mass-loss/activity relation (see Figure 1.8). Clearly more stars must be studied, especially the more active stars, to determine whether or not the apparent cutoff line near X-ray surface flux 10^6 ergs cm^{-2} s^{-1} is real and what the mass-loss/activity relation might be for even more active stars. If the cutoff is real, then it may indicate a difference in the coronal magnetic field configuration of highly active stars compared to less active stars. We are presently searching the *HST* archive for suitable stars to analyze but new observations are clearly needed to better determine the mass-loss/activity relation for stars with F_x both below and above the apparent cutoff near 10^6 ergs cm^{-2} s^{-1}.

Schrijver and Title (2001) have computed surface magnetic field structures for solar-like stars that assume the same magnetic flux injection and surface distribution properties as the present day Sun but higher rates for the emergence of magnetic fields that would correspond to a faster rotating Sun with an enhanced magnetic dynamo. They find that for a solar-like star with a rotation period of 6 days (rotating about 4 times faster than the Sun), the total unsigned magnetic flux on the stellar surface is 10 times that of the Sun at solar maximum. This star develops a large magnetic polar spot with an opening angle of 25°, and the astrosphere has a predominately magnetic dipole geometry. Active stars of all types, including RS CVn systems (like λ And), young GK stars, M dwarfs, and T Tauri stars, show evidence for polar spots (cf. Schrijver et al. 2003). Since the X-ray surface flux is roughly proportional to the magnetic flux density (cf. Schrijver et al. 2003) and the X-ray luminosity of the active Sun in the soft X-ray ROSAT band is about 4.7×10^{27} erg cm^{-2} s^{-1} (Peres et al. 2000), the model active star with a 6-day rotational period would have a surface X-ray flux $F_x \approx 7.6 \times 10^5$ erg cm^{-2} s^{-1}. Thus the proposed cutoff line in Figure 1.8 occurs at about the same X-ray surface flux as the appearance (both in observations and in the models) of large polar spots and strong astrospheric magnetic fields with a dipole geometry that could suppress mass loss over most of the stellar surface.

2.2 The Mass-Loss History of the Sun

The empirical relation between the mass-loss rate and the X-ray surface flux (F_x) shown in Figure 1.8 for $F_x \leq 10^6$ ergs cm^{-2} s^{-1} is

$$\dot{M} \propto F_x^{1.15\pm0.20}. \tag{1.1}$$

We can now use the known relation between stellar age and activity (e.g., Ayres 1997) to infer the dependence of mass-loss rate on stellar age. As stars age, their rotation rates (V_{rot}) slow due to magnetic braking and their X-ray fluxes decrease. There are many empirical relations decribing this evolution of stellar activity. We adopt the empirical relations of Ayres (1997),

$$V_{rot} \propto t^{-0.6\pm0.1}, \tag{1.2}$$

and

$$F_x \propto V_{rot}^{2.9\pm0.3}. \tag{1.3}$$

Combining these three relations (see Wood et al. 2002), we obtain

$$\dot{M} \propto t^{-2.00\pm0.52}. \tag{1.4}$$

This relation predicts that when the young Sun ($t \approx 10^8$ years) had saturated X-ray emission ($L_x/L_{bol} = 10^{-4}$), its mass-loss rate was 200–10,000 times larger than at present. The cumulative mass loss from age 10^8 years to the present is $\leq 0.03 M_\odot$ (see Figure 1.10).

The mass-loss history of the Sun (Figure 1.9) predicts that the wind of the young Sun was roughly 1000 times stronger than at present. In addition to its obvious importance for solar and stellar astronomy, this result may have very important ramifications for planetary science as well, since solar wind erosion may have played an important role in the evolution of planetary atmospheres, especially that of Mars (e.g., Kass & Yung 1995). However, the existence of a high-activity cutoff in Figure 1.8 would mean that the solar wind evolution law shown in Figure 1.9 would only apply for $t > 0.7$ Gyr, and that at earlier times the solar wind may have actually been very weak.

Given the importance of these results to both solar and stellar astronomy and to planetary science, we believe it is crucial to test and refine these results with new astrospheric detections. The mass-loss rates measured from the detected astrospheric Lyman-α absorption should also be verified using astrospheric models other than the presently used four-fluid models, preferably kinetic models such as those of Baranov & Malama (1993, 1995). Once we have a heliospheric model that can successfully match the HST heliospheric data, then we can extrapolate from it astrospheric models assuming different mass-loss rates, compare these results with the astrospheric Lyman-α data, and determine whether or not the mass-loss rates that we derive are consistent with those listed in Table 1.3 from Wood et al. (2002).

3. Influence of Stellar Winds on Planets in the Solar System and Beyond

Equation (1.4) provides us with the ability to make quantitative estimates of the solar wind flux that planets received during the early solar system. This is important for addressing such questions as (i) why the young Earth had running water when the Sun was 25% fainter than today and (ii) whether solar wind erosion removed water from the young Martian atmosphere. Exposure to a stellar wind, together with UV and X-ray irradiation, can ionize and erode planetary atmospheres, and the higher mass-loss rates suggested for the young Sun and young stars with high X-ray fluxes would exacerbate these effects. Solar wind sputtering processes have been proposed to have important effects on the atmospheres of Venus and Titan, but Mars may be the most interesting case of solar wind erosion, since the history of its atmosphere is linked to whether or not water, and perhaps life, once existed on the surface.

Unlike Earth, the Martian atmosphere is not currently protected from the solar wind by a strong magnetosphere. There is evidence that Mars once had a magnetic field, which disappeared at least 3.9 Gyr ago (Acuña et al. 1999). At that time, the Martian atmosphere would have been directly exposed to a solar wind about 40 times stronger than the current wind. This would have had a dramatic effect on its atmosphere through ion-pickup and sputtering processes.

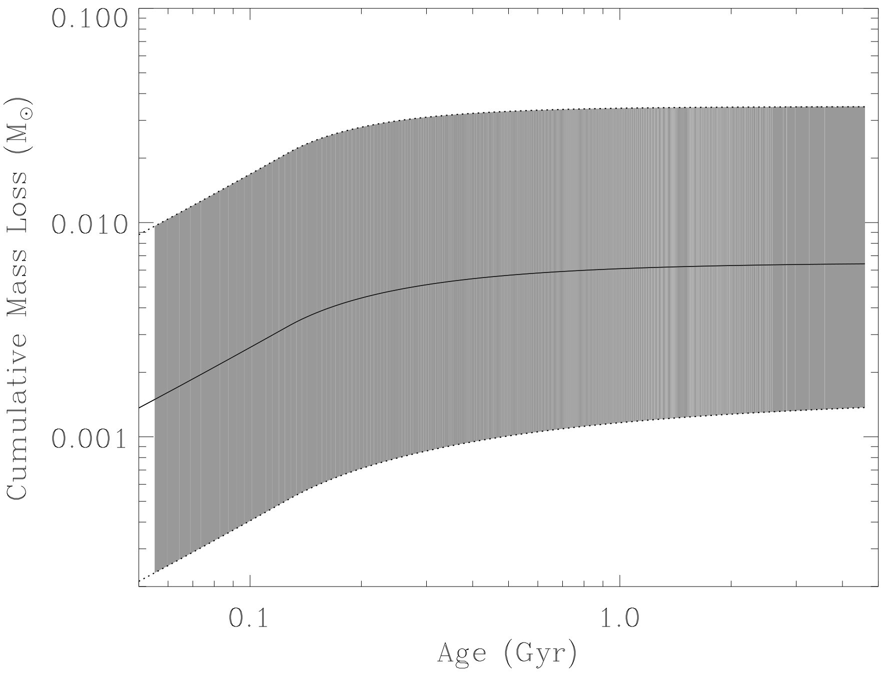

Figure 1.10. Cumulative mass loss for the Sun as a function of time, based on the mass-loss history of the solar wind in Figure 1.9.

Mars appears to have had running water on its surface in the distant past and a thicker atmosphere that could have supported a climate consistent with the existence of surface water (e.g., Jakosky & Phillips 2001). Solar wind erosion and XUV radiation are leading candidates for the cause of its present thin atmosphere and lack of surface water (e.g., Lundin 2001; Lammer et al. 2003). Planets around other stars could have similar histories.

4. Conclusions

- Analysis of the astrospheric absorption features seen in the Lyman-α lines toward nearby stars provides the first quantitative measurements of mass-loss rates for G and K dwarf stars.

- We find that the mass-loss rates increase with activity, as measured by the X-ray surface flux, and thus with decreasing stellar age. More *HST/STIS* spectra are needed to determine whether an important change in mass-loss rates occures near $F_x \approx 10^6$ ergs cm^{-2} s^{-1}.

- The mass-loss rate for the Sun at 10^8 years is predicted to be 200–10,000 times larger than at present and likely played a major role in the evolution of planetary atmospheres.

We thank NASA and the Space Telescope Science Institute for grants to the University of Colorado and NSF for its support. We also thank Dr. Hans-Reinhard Müller and Prof. Gary Zank for their assistance in computing the astrosphere models. We also than Dr. Steven Suess and the referee for their careful reading of the manuscript and their helpful suggestions.

References

Acuña, M.J. et al. 1999, Science, 284, 790.
Ayres, T.R. 1997, JGR, 102, 1641.
Ayres, T.R., Brown, A., Osten, R.A., Huenemoerder, D.P., Drake, J.J., Brickhouse, N.S., and Linsky, J.L. 2001, ApJ, 549, 544.
Ayres, T.R., Brown, A., Harper, G.M., Osten, R.A., Linsky, J.L., Wood, B.E., and Redfield, S. 2003, ApJ, 583, 963.
Baranov, V.B. & Malama, Y.G. 1993, JGR, 98, 15157.
Baranov, V.B. & Malama, Y.G. 1995, JGR, 100, 14755.
Biermann, L. 1951, Zeitschrift für Astrophysik, 29, 274.
Deutsch, A.J. 1956, ApJ, 123, 210.
Dring, A. R., Linsky. J., Murthy, J., Henry, R. C., Moos, W., Vidal-Madjar, .A., Audouze, J., & Landsman, W. 1997, ApJ, 488, 760.
Jakosky, B.M. & Phillips, R.J., 2001, Nature, 412, 237.
Gayley, K. G., Zank, G. P., Pauls, H. L., Frisch, P. C., & Welty, D. E. 1997, ApJ, 487, 259.
Izmodenov, V. V., Gruntman, M., & Malama, Y. G. 2001, JGR, 106, 10681.
Izmodenov, V. V., Lallement, R., & Malama, Y. G. 1999, A&A, 342, 113.
Izmodenov, V. V., Wood, B. E., & Lallement, R. 2002, JGR, 107, 1308.
Kass, D. M., & Yung, Y. L. 1995, Science, 268, 697.
Lamers, H.J.G.L.M. & Cassinelli, J.P. 1999, *Introduction to Stellar Winds*. Cambridge: Cambridge University Press.
Lammer, H. et al. 2003, Icarus, 165, 9L.
Landsman, W.B., Henry, R.C., Moos, H.W., & Linsky, J.L. 1984, ApJ, 285, 801.
Lallement, R., Ferlet, R., Lagrange, A. M., Lemoine, M., & Vidal-Madjar, A. 1995, A&A, 304, 461.
Linde, T., Gombosi, T. I., Roe, P. L., Powell, K. G., & DeZeeuw, D. L. 1998, JGR, 103, 1889.
Linsky, J.L. et al. 1993, ApJ, 402, 694.
Linsky, J.L. et al. 1995, ApJ, 451, 335.
Linsky, J.L. & Wood, B.E. 1996, ApJ, 463, 254.

Lundin, R. 2001, Science, 291, 1909.
Müller, H. -R., Zank, G. P., & Lipatov, A. S. 2000, JGR, 105, 27419.
Müller,. H. -R., Zank, G. P., & Wood, B. E. 2001a, ApJ, 551, 495.
Müller,. H. -R., Zank, G. P., & Wood, B. E. 2001b, in The Outer Heliosphere: The Next Frontiers, ed. K. Scherer et al. (Amsterdam: Pergamon), 53.
Opher, M., Liewer, P. C, Gombosi, T. I., Manchester, W., DeZeeuw, D. L., Sokolov, I., & Toth, G. 2003, ApJ, 591, 161.
Parker, E.N. 1958, ApJ, 128, 664.
Parker, E.N. 1960, ApJ, 132, 821.
Peres, G., Orlando, S., Reale, F., Rosner, R., & Hudson, H. ApJ, 528, 537.
Phillips, J.L., Bame, S.J., Feldman, W.C., Goldstein, B.E., Gosling, J.T., Hammond, C.M., McComas, D.J., Neugebauer, M., Scime, E.E., & Suess, S.T. 1995, Science, 268, 1030.
Pauls, H. L., Zank, G. P., & Williams, L. L. 1995, JGR, 100, 21595.
Ratkiewicz, R., Barnes, A., Molvik, G. A., Spreiter, J. R., Stahara, S. S., Vinokur, M., & Venkateswaran, S. 1998, A&A, 335, 363.
Redfield, S., Ayres, T.R., Linsky, J.L., Ake, T.B., Dupree, A.K., Robinson, R.D., and Young, P.R. 2003, ApJ, 585, 993.
Schrijver, C.J., & Title, A.M., ApJ, 551, 1099.
Schrijver, C.J., DeRosa, M.L., & Title, A.M., ApJ, 590, 493.
Witte, M., Rosenbauer, H., Banaszkewicz, M., & Fahr, H. 1993, Adv. Space Res., 13, 121.
Wood, B.E. & Linsky, J.L. 1996, ApJ, 470, 1157.
Wood, B.E. & Linsky, J.L. 1998, ApJ, 492, 788.
Wood, B. E., Alexander, W. R., & Linsky, J. L. 1996, ApJ, 470, 1157.
Wood, B. E.., Linsky, J. L., & Zank, G. P. 2000a, ApJ, 537, 304
Wood, B. E., Muller, H. -R., & Zank, G. P. 2000b, ApJ, 542, 493.
Wood, B.E. et al. 2001, ApJ, 547, L49.
Wood, B.E. et al. 2002, ApJ, 574, 412.
Zank, G.P. et al. 1996, JGR, 101, 21639.